HHS Public Access

Author manuscript

Nat Commun. Author manuscript; available in PMC 2015 March 03.

Published in final edited form as:

Nat Commun. ; 5: 4642. doi:10.1038/ncomms5642.

Early-onset metabolic syndrome in mice lacking the intestinal uric acid transporter *SLC2A9*

Brian J. DeBosch,

BJC Institute of Health, Washington University School of Medicine 10th Floor 425 S. Euclid Avenue Campus Box 8064 St. Louis MO 63110

Oliver Kluth,

Department of Experimental Diabetology, German Institute of Human Nutrition Potsdam-Rehbruecke, Nuthetal 14558

Hideji Fujiwara,

BJC Institute of Health, Washington University School of Medicine 10th Floor 425 S. Euclid Avenue Campus Box 8064 St. Louis MO 63110

Annette Schürmann, and

Department of Experimental Diabetology, German Institute of Human Nutrition Potsdam-Rehbruecke, Nuthetal 14558

Kelle Moley

BJC Institute of Health, Washington University School of Medicine 10th Floor 425 S. Euclid Avenue Campus Box 8064 St. Louis MO 63110

Abstract

Excess circulating uric acid, a product of hepatic glycolysis and purine metabolism, often accompanies metabolic syndrome. However, whether hyperuricemia contributes to development of metabolic syndrome or is merely a by-product of other processes that cause this disorder has not been resolved. Additionally, how uric acid is cleared from the circulation is incompletely understood. Here, we present a genetic model of spontaneous, early-onset metabolic syndrome in mice lacking the enterocyte urate transporter Glut9 (encoded by the *SLC2A9* gene). Glut9-deficient mice develop impaired enterocyte uric acid transport kinetics, hyperuricemia, hyperuricosuria, spontaneous hypertension, dyslipidemia, and elevated body fat. Allopurinol, a xanthine oxidase inhibitor, can reverse the hypertension and hypercholesterolemia. These data provide evidence that hyperuricemia *per se* could have deleterious metabolic sequelae. Moreover, these findings suggest that enterocytes may regulate whole-body metabolism, and that enterocyte urate metabolism could potentially be targeted to modulate or prevent metabolic syndrome.

Correspondence and requests for materials should be addressed to moleyk@wudosis.wustl.edu.

Author Contributions

BJD designed, executed and interpreted experiments, and wrote the manuscript. OK and AS designed, executed and interpreted experiments and generated the floxed Glut9 model. HF designed, executed and interpreted the LC/MS experiments. KHM designed and interpreted experiments and critically reviewed the paper.

Competing financial interest

The authors have no competing financial interests to disclose.

INTRODUCTION

Metabolic syndrome is a complex multifactorial disease that afflicts two in five adults in the U.S. alone[1], and scores more worldwide. Observations over the prior two decades demonstrated increased metabolic syndrome, type 2 diabetes mellitus and cardiovascular morbidity in hyperuricemic subjects[3-4], and that serum uric acid levels independently predict diabetes, fatty liver and metabolic syndrome[3]. Work in rodent models further mechanistically implicated uric acid in fructose-induced metabolic syndrome[5], although some controversy over the exact physiological function of urate (the predominant form of uric acid at physiological pH) remains[8,9]. Elucidating how urate is removed from the circulation may nevertheless have broad individual and public health implications.

Approximately 60-70% of circulating uric acid clearance occurs in the kidney and the other 30-40% is cleared via intestinal enterocytes[6], although the enterocyte may become the primary excretory pathway in renally insufficient patients[10] (e.g. in patients with diabetes, hypertension or cardiorenal disease). Recent data suggest that defective extrarenal clearance is a common cause of hyperuricemia[11], yet few studies address enterocyte urate handling mechanisms[11-13], and none address endogenous urate clearance mechanisms as effectors of mammalian metabolism. The putative enterocyte urate transporters – BCRP/ABCG2 (and potentially SLC17A4/NPT5) are apical transporters[12,13], whereas a basolateral transporter has not been identified. Therefore, it was unresolved how uric acid flux occurred down its gradient from the blood into the enterocyte cytoplasm prior to excretion in the stool.

Recent data in humans and in rodents identified GLUT9/Glut9 as a high-capacity urate transporter[14,15], the deletion of which alters urate homeostasis in a tissue-specific manner[16-17]. Furthermore, Glut9 is a basolateral and apical membrane transporter in other polarized epithelial cell types[14]. Thus, we examined GLUT9 localization, cellular function and role in urate homeostasis in the murine intestine.

Here, we show that Glut9 is localized to the apical and basolateral enterocyte membranes, and that enterocyte-specific Glut9 deficiency impairs enterocyte urate transport. Concomitant with these urate clearance defects, enterocyte Glut9-deficient mice develop hyperuricemia, hyperuricosuria and early-onset metabolic syndrome - hypertension, dyslipidemia, hyperinsulinemia and hepatic fat deposition - which is partly mitigated by *ad lib* administration of the xanthine oxidase inhibitor, allopurinol. These results suggest that Glut9 regulates enterocyte urate clearance, and that enterocyte Glut9 deficiency may have deleterious metabolic sequelae.

RESULTS

Expression and localization of enterocyte Glut9

Immunoblot analysis demonstrated that Glut9 was abundantly expressed in intestine (Fig. 1A), highly in the jejunum and ileum (Fig. 1B), the segments of the intestine that perform the majority of urate excretion[10,12]. Confocal immunofluorescence microscopy of fixed mouse intestine revealed Glut9 localized predominantly to the basolateral enterocyte membrane with some apical staining (Fig. 1C).

Generation of mice lacking enterocyte Glut9

Given that Glut9 is the only reported basolateral urate transporter, we hypothesized that mice lacking Glut9 in enterocytes would have impaired enteric urate handling. We thus generated enterocyte-specific Glut9-deficient mice by crossing mice harboring a floxed *SLC2A9* allele with mice overexpressing *cre* recombinase driven by the enterocyte-specific *villin* promoter (Figs. 1D and 1E). *vil*-Cre / *SLC2A9*$^{fl/fl}$ (G9EKO) mice were live-born in Mendelian ratios, were fertile, and had no gross morphologic defects (Table 1). Immunoblotting confirmed deficiency of total Glut9A and total Glut9 protein in G9EKO small bowel lysates (Fig. 1F and Supplementary Figs. 1 and 2). Isolated villous enterocytes from G9EKO mice exhibited a ~65% [^{14}C]-urate uptake defect versus WT enterocytes when compared with mice expressing *vil*-Cre with wild-type *SLC2A9* alleles (hereafter referenced as “WT” mice) (Fig. 1G). Congruent with these findings, liquid chromatography-mass spectrometry (LC/MS) of stool extracts revealed significantly decreased stool urate concentrations in G9EKO mice versus WT mice (Fig. 1H). Together, these results suggested impaired enterocyte uptake and efflux into stool in G9EKO animals.

Physiological consequences of impaired enterocyte urate clearance

We next examined physiological consequences of impaired enterocyte urate efflux in mice fed standard rodent chow (Picolab # 5053: 25% protein, 13% fat and 62% carbohydrate). Uricase-based urate determinations further revealed significantly higher uric acid concentrations in both serum and urine in G9EKO mice (Fig 2A and 2B). Body composition analysis by EchoMRI revealed significantly elevated body fat mass and fat percentage (Fig. 2C and 2D) despite higher resting energy expenditure as determined by indirect calorimetry in G9EKO mice (Table 2). Plasma analysis revealed G9EKO mice had significantly elevated total cholesterol, free fatty acids and triglycerides (Fig. 2E, 2F, 2G). Some evidence of early insulin resistance was observed, with an approximately 40% elevation in fasting plasma insulin in G9EKO mice (Fig. 2H) in context of normal fasting blood glucose (Fig. 2I) and insulin tolerance testing (Fig. 2J). Tail-cuff plethysmography in unanesthetized G9EKO mice demonstrated significant baseline hypertension when compared with WT mice (Fig. 2K).

We next assessed whether blocking uric acid production could reverse any of these effects of impaired urate clearance. WT and G9EKO mice were thus exposed to 8-weeks allopurinol (150 mg/L) *ad libitum* in sterilized drinking water approximately 4-weeks after weaning[5]. Plasma uric acid was significantly decreased in G9EKO mice following allopurinol treatment without significant effects on urine urate concentrations (Fig. 3A and 3B). Strikingly, in comparison to untreated G9EKO mice, allopurinol treatment also lowered blood pressure and total cholesterol (Fig. 3C and 3D) without significant effects on free fatty acids and triglycerides suggesting at least partial allopurinol-reversibility of the spontaneous metabolic syndrome in G9EKO mice - either through xanthine oxidase inhibition or through direct effects on renal uric acid transporters by allopurinol or by its active metabolite, oxypurinol. Fasting FFA and TG were not significantly affected by allopurinol (Fig. 3E and 3F).

We then looked at well-described secondary complications of hyperuricemia in G9EKO mice, including non-alcoholic fatty liver disease and cardiovascular disease. Consistent with findings of increased steatosis / NAFLD in patients with hyperuricemia[18], hepatic triglycerides and free fatty acids were elevated in G9EKO livers versus WT livers (Fig. 4A and 4B). Additionally, mRNA for sterol regulatory element-binding protein, a marker of cholesterol metabolism, was significantly elevated in the livers of G9EKO mice, and there was a trend toward elevated Collagen Type 1 alpha and fatty acid synthase, markers of fibrosis and fat synthesis.

The increased incidence of cardiovascular morbidity in hyperuricemic patients prompted us to survey the cardiac phenotype of G9EKO mice. Basal heart rate observed by echocardiography was significantly elevated in G9EKO mice (Fig. 4D). Echocardiogram also revealed evidence of cardiac hypertrophic remodeling, (Fig. 4E and 4F) – decreased diastolic left ventricular internal diameter with increased relative wall thickness – a common finding in patients with hyperuricemia[19]. However, although allopurinol treatment significantly lowered body weight (Fig. 5A) and hepatic triglyceride content (Fig. 5C) associated with a trend toward lower body fat mass in G9EKO mice (Fig. 1B), allopurinol treatment did not significantly reverse the G9EKO-associated changes in heart rate, left ventricular internal diameter or relative wall thickness (Fig. 5D, 5E and 5F).

DISCUSSION

Mice lacking enterocyte Glut9 thus develop early-onset spontaneous hyperuricemic metabolic syndrome that is partially mitigated by allopurinol, a xanthine oxidase inhibitor. Not all deleterious findings in the G9EKO model were reversed by allopurinol, suggesting either a) some metabolic syndrome components occur independently of hyperuricemia, b) some metabolic syndrome components caused by hyperuricemia are irreversible once clinically apparent, or c) uric acid is unrelated to any findings, and the allopurinol effects are derived specifically from blocking oxidant production via xanthine oxidase inhibition *per se*. It should be noted, however, that the key advantage to this model of impaired urate excretion in delineating the specific effects of hyperuricemia is that it does not rely upon xanthine oxidase activity to produce hyperuricemia as in some of the diet-induced models (e.g. fructose- or purine-rich diets). Nevertheless, while further insight into the effects of hyperuricemia on its host are required, the G9EKO model suggests that attenuated enterocyte urate clearance could be a critical, initiating step in metabolic syndrome pathogenesis. Interdicting circulating urate accumulation by focusing on gut urate reuptake and clearance could represent a novel treatment paradigm to block or modulate hyperuricemia and its complications, including metabolic syndrome. We expect this model can now be used to probe mechanistically into the role of urate in the complications and sequelae of metabolic syndrome.

METHODS

Generation of G9EKO Mice

Enterocyte-specific Glut9-deficient mice were generated by homologous recombination of the 18.9kb targeting vector harboring loxP sites flanking exons 5 and 6 and a neomycin

resistance cassette 3' of exon 6. Modified embryonic stem cells from 129Sv mice carrying this targeting allele were introduced into C57BL/6 blastocysts. Chimeric offspring were twice backcrossed into the C57BL/6 line to generate N2 mice heterozygous for the targeting allele (genotype *Slc2a9*$^{fl/+}$). N2 mice were intercrossed to generate homozygous (*Slc2a9*$^{fl/fl}$) mice. Genotyping primers were as follows (listed 5' – 3'): Forward primer – TGGTGCTACTCTGTGGTGCTA. Reverse primer – CACAGCGGTGAAAGTAACGA. Mice harboring homozygous floxed *Slc2a9* alleles were crossed with mice expressing Cre recombinase under the mouse villin 1 promoter on a C57/BL6 background (Jackson Laboratories, stock number 004586) to generate G9EKO mice. Mice expressing villin promoter-driven Cre with wild-type *Slc2a9* alleles were used as control mice throughout these studies. For allopurinol treatment experiments, 8 week-old mice were maintained on 150 mg/L allopurinol[5] for 8 weeks prior to metabolic characterization. All animal procedures were approved by the Washington University School of Medicine Animal Studies Committee.

Calorimetry body composition & blood pressure determination

Indirect calorimetry, echoMRI and blood pressure analyses on unanesthetized mice were performed via the Mouse Diabetic Models Phenotyping Core Facility at Washington University using an Oxymax Indirect Calorimeter (Columbus Instruments, Columbus, OH), an EchoMRI 3– 1 (Echo Medical Systems, Houston, TX[20-21], and a Columbus Instruments NIBP (Columbus, OH) tail-cuff and plethysmograph. Food consumed in mice was measured in 24-hour increments during each calorimetry run.

Radiolabeled uric acid uptake measurements

Apical villous enterocytes first were enriched by calcium chelation and mechanical disruption[22]. Briefly, sections of distal jejunum (5–6 cm) were removed, flushed with ice-cold phosphate-buffered saline, and opened longitudinally prior to immersion in ice-cold phosphate-buffered saline. The bowel was transferred into 5 mL ice-cold BSS buffer (1.5 mM KCl, 96 mM NaCl, 27 mM sodium citrate, 8 mM KH_2PO_4, 5.6 mM Na_2HPO_4, 15 mM EDTA, and 1 mM dithiothreitol) and vortexed at 4 °C at maximum speed for 20 min. Following this step, almost all epithelial cells were recovered in the BSS solution. The BSS solution (containing crypts and villi) was filtered through a 70-μm cell strainer (BD Biosciences, San Jose, CA)). The larger size villi were captured in the cell strainer whereas crypts were discarded in the effluent. Crypt fractions were then spun down at 1000 × *g* for 10 min at 4 °C and washed once with Tris buffer (150 mM NaCl, 1 mM EDTA, 1 mM EGTA, 50 mM Tris-HCl, pH 8.0) then with ice-cold DMEM prior to assay. To assay uptake, cells were resuspended in pre-warmed, 37 °C DMEM containing 1 μCi mL^{-1} [^{14}C]-uric acid (American Radiolabeled Chemicals, St. Louis, MO) for 3 minutes prior to quenching and 3 wash steps in ice-cold HBSS. Samples were subjected to liquid scintillation counting and counts were normalized to sample protein, as determined by BCA assay kit (Pierce, Rockford, IL).

Western Blotting and Immunostaining

Western blotting was performed using 50-100 μg protein subjected to 10% SDS-PAGE, followed by transfer to nitrocellulose membrane and overnight primary antibody incubation[24-25] (1:1000 dilutions at 4°C) with the following antisera: total Glut9, GAPDH (clone 14C10, Cell Signaling Technologies, Beverly MA), Glut9A[14] Actin (clone C4, EMD Millipore, Billerica, MA). Fixed (4% paraformaldehyde), paraffin-embedded intestinal sections were sectioned, permeablized in 0.1% triton X-100 in phosphate-buffered saline and blocked with 2% bovine serum albumin (Sigma-Aldrich, St. Louis, MO) prior to immunostaining using pre-immune serum or GLUT9-specific antibody (Generated in the laboratory of Dr. Annette Schürmann) at a 1:200 dilution.

Liquid chromatography and tandem mass spectrometry

Uric acid analysis in stool was performed by the Washington University Metabolomics Facility. Uric acid was extracted from ~20 mg dried, pulverized, sieved mouse stool using water containing 1-methyluric acid (Sigma) for LC/MS/MS using a modified US analysis method[25]. 1-methyluric acid was chosen as the internal standard and a Thermo betasil LC column was used for negative ion electrospray LC/MS/MS analysis.

Hepatic Lipid Extraction

Hepatic lipids were extracted by homogenizing 100 mg liver tissue in 2 mL (2:1) chloroform:methanol[23]. Remaining tissue was pelleted by centrifugation and 10-20 μL supernatant aliquots were dried for two hours prior to resuspension in assay reagent. Values were normalized to tissue input mass.

Biochemical analyses

Serum and urine uric acid, serum and hepatic cholesterol, TG, FFA and serum insulin were measured using the following kits precisely per manufacturer instructions[20,21,23]: Amplex Red Uric Acid Assay Kit (Invitrogen, Carlsbad, CA), Infinity Cholesterol Assay Kit, (Thermo Scientific, Waltham, MA), Infinity triglyceride assay kit (Thermo Scientific, Waltham, MA), NEFA free fatty acid determination kit (Wako Diagnostics, Richmond, VA) and rat / mouse insulin ELISA assay kit (Millipore, Billerica, MA).

Echocardiography

Echocardiography was performed by the Washington University Mouse Cardiovascular Phenotyping Core Facility[24]. Non-invasive transthoracic cardiac ultrasound exams were performed under light general anesthesia using a VisualSonics Vevo 2100 cardiac echocardiography machine with a 15MHz linear transducer.

Statistical Analysis

All values are expressed as the mean ± SEM. Two-tailed T-tests were applied with Bonnferroni-Dunn *post hoc* correction for multiple comparisons. $P < 0.05$ was considered to be statistically significant between groups.

Supplementary Material

Refer to Web version on PubMed Central for supplementary material.

Acknowledgements

The authors thank Nicole Junicke for technical work in generating the targeting vector used to produce the G9EKO mouse line. This work was supported by the Pediatric Scientist Development Program (PSDP) NIH grant 5K12HD000850-27 (to BJD), DDRCC grant P30DK52574 (to BJD), and R01HD040390-07 (KHM). The German Ministry of Education and Research (BMBF: DZD, 01GI0922), and the State of Brandenburg (to AS and OK). The Washington University Mouse Diabetes Model Phenotyping Core is supported by DRTC grant P60 DK020579. Mass spectrometry was performed in the Metabolomics Facility at Washington University (P30 DK020579).

REFERENCES

1. Alberti, KG., et al. Circulation. Vol. 120. National Heart, Lung, and Blood Institute; American Heart Association; World Heart Federation; International Atherosclerosis Society; and International Association for the Study of Obesity; 2009. Harmonizing the metabolic syndrome: a joint interim statement of the International Diabetes Federation Task Force on Epidemiology and Prevention; p. 1640
2. Arden C, et al. Elevated Glucose Represses Liver Glucokinase and Induces Its Regulatory Protein to Safeguard Hepatic Phosphate Homeostasis. Diabetes. 2011; 60:3110. [PubMed: 22013014]
3. Johnson RJ, et al. Sugar, uric acid, and the etiology of diabetes and obesity. Diabetes. 2013; 62:3307. [PubMed: 24065788]
4. Feig DI, Kang DH, Johnson RJ. Uric acid and cardiovascular risk. N Engl J Med. 2008; 359:1811. [PubMed: 18946066]
5. Nakagawa T, et al. A causal role for uric acid in fructose-induced Metabolic Syndrome. Am J Physiol Renal Physiol. 2006; 290:F625. [PubMed: 16234313]
6. So A, Thorens B. Uric acid transport and disease. J Clin Invest. 2010; 120:1791. [PubMed: 20516647]
7. Choi H, Ford ES. Prevalence of the metabolic syndrome in individuals with hyperuricemia. Am J Med. 2007; 120:442. [PubMed: 17466656]
8. Palmer TM, et al. Association of plasma uric acid with ischaemic heart disease and blood pressure: mendelian randomisation analysis of two large cohorts. BMJ. 2013; 347:f4262. [PubMed: 23869090]
9. Hughes K, et al. Mendelian randomization analysis associates increased serum urate, due to genetic variation in uric acid transporters, with improved renal function. Kidney Int. 2014; 85:344. [PubMed: 24048376]
10. Sorensen LB. Role of the intestinal tract in the elimination of uric acid. Arthritis Rheum. 1965; 8:694. [PubMed: 5859543]
11. Ichida K, et al. Extra-renal urate excretion is a common cause of hyperuricemia. Nature Communications. 2012; 3:764.
12. Hosomi A, Nakanishi T, Fujita T. Tamai I Extra-Renal Elimination of Uric Acid via Intestinal Efflux Transporter BCRP/ABCG2. PLoS ONE. 2012; 7:e30456. [PubMed: 22348008]
13. Anzai N, Endou H. Urate transporters: an evolving field. Semin Nephrol. 2011; 31:400. [PubMed: 22000646]
14. Augustin R, et al. Identification and characterization of human glucose transporter-like protein-9 (Glut9): alternative splicing alters trafficking. J Biol Chem. 2004; 279:16229. [PubMed: 14739288]
15. Caulfield MJ, et al. SLC2A9 Is a High-Capacity Urate Transporter in Humans. PLoS Med. 2008; 5:e197. [PubMed: 18842065]
16. Preitner F, et al. Glut9 is a major regulator of urate homeostasis and its genetic inactivation induces hyperuricosuria and urate nephropathy. Proc Natl Acad Sci. 2009; 106:15501. [PubMed: 19706426]

17. Preitner F, et al. Urate-induced acute renal failure and chronic inflammation in liver-specific Glut9 knockout mice. Am J Physiol Renal Physiol. 2013; 305:F786. [PubMed: 23804456]
18. Katsiki N, Athyros VG, Karagiannis A, Mikhailidis DP. Hyperuricaemia and non-alcoholic fatty liver disease (NAFLD): a relationship with implications for vascular risk? Curr Vasc Pharmacol. 2011; 9:698. [PubMed: 21388346]
19. Kurata A, Shigamatsu Y, Hikagi J. Sex-related differences in relations of uric acid to left ventricular hypertrophy and remodeling in Japanese hypertensive patients. Hypertension Research. 2005; 28:133. [PubMed: 16025740]
20. DeBosch BJ, Chi M, Moley KH. Glucose Transporter 8 (GLUT8) Regulates Enterocyte Fructose Transport and Global Mammalian Fructose Utilization. Endocrinology. 2012; 153:4181. [PubMed: 22822162]
21. DeBosch BJ, Chen Z, Finck BN, Chi M, Moley KH. Glucose transporter 8 (GLUT8) mediates glucose intolerance and dyslipidemia in high-fructose diet-fed male mice. Mol Endocrinol. 2013; 27:1887. [PubMed: 24030250]
22. Sun RC, Choi PM, Guo J, Erwin CR, Warner BW. Insulin-like growth factor 2 and its enterocyte receptor are not required for adaptation in response to massive small bowel resection. J Ped Surg. 2014; 49:966.
23. DeBosch BJ, Chen Z, Saben JL, Finck BN, Moley KH. Glucose transporter 8 (GLUT8) mediates fructose-induced de novo lipogenesis and macrosteatosis. J Biol Chem. 2014; 289:10989. [PubMed: 24519932]
24. DeBosch B, et al. Akt1 is required for physiological cardiac growth. Circulation. 2006; 113:2097. [PubMed: 16636172]
25. Kim KM, et al. J. Chromatogr B Analyst Technol Biomed Life Sci. 2009; 877:2032–2038.

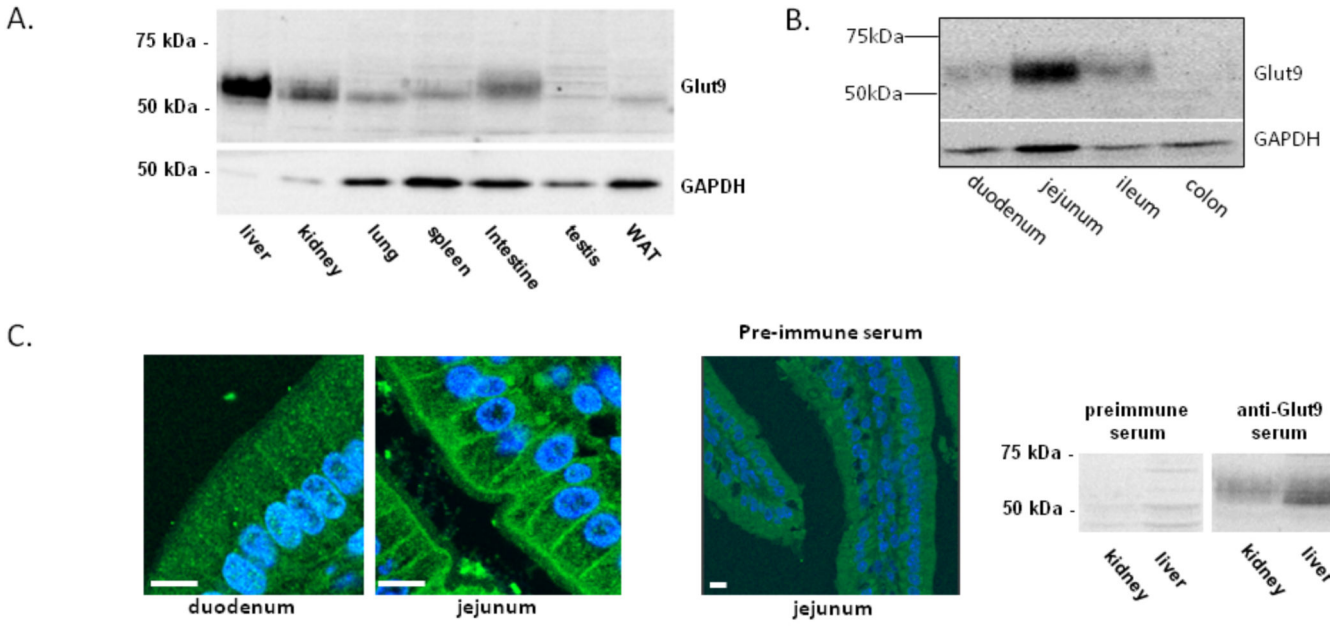

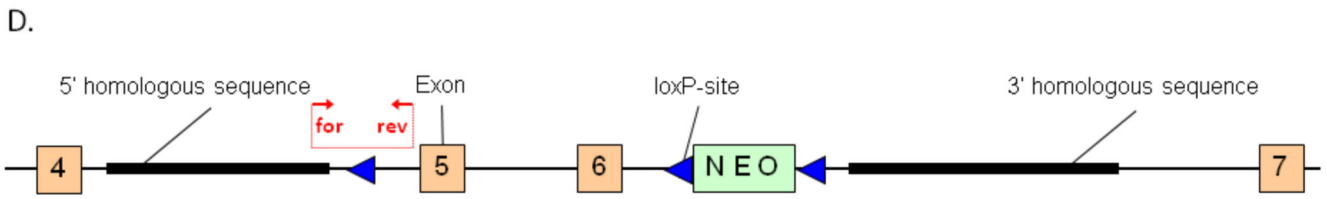

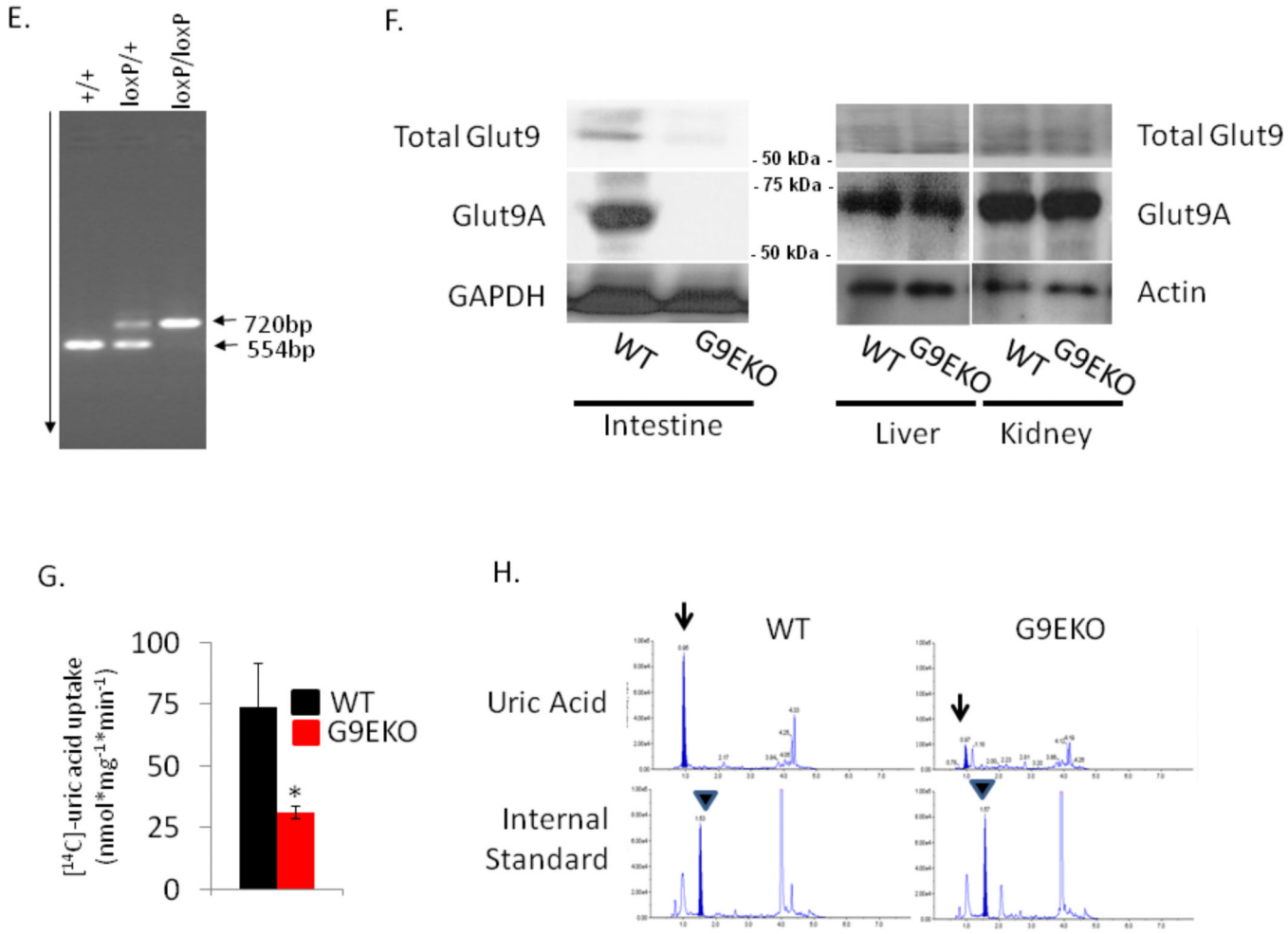

Figure 1.

Characterization of intestinal Glut9 and genetic deletion of enterocyte SLC2A9. A. Immunoblotting against full-length Glut9 in murine tissue. B. Small bowel segment-specific Glut9 immunoblotting. C. Left, confocal immunofluorescence microscopy demonstrating basolateral and apical Glut9 localization in duodenum and jejunum. Middle, jejunal immunostaining with pre-immune serum. Scale bars, 10 μm. Right, specificity of total Glut9 antiserum versus pre-immune serum by liver and kidney lysate immunoblotting D. Glut9 targeting construct used to generate mice harboring floxed *SLC2A9* flanking exons 5 and 6. Forward and reverse (for/rev) genotyping primers flank the flox site adjacent to exon 5. E. PCR bands depicting larger floxed (720bp) and wild-type (554bp) sequences. F. Immunoblot of Glut9A in WT and G9EKO mouse whole intestine, liver and kidney lysate. G. [^{14}C]-uric acid uptake in purified villous enterocyte fractions from WT and G9EKO mice. n = 5 per group. In vitro experiment replicated thrice. *, $P < 0.05$ vs. WT [2-tailed T-testing] Error bars represent standard error of the mean (SEM) H. LC/MS analysis of stool from WT and G9EKO mice. Upper spectra – uric acid (arrows) elution. Lower spectra (arrowheads) – 1-methyluric acid internal standard. Experiment replicated thrice.

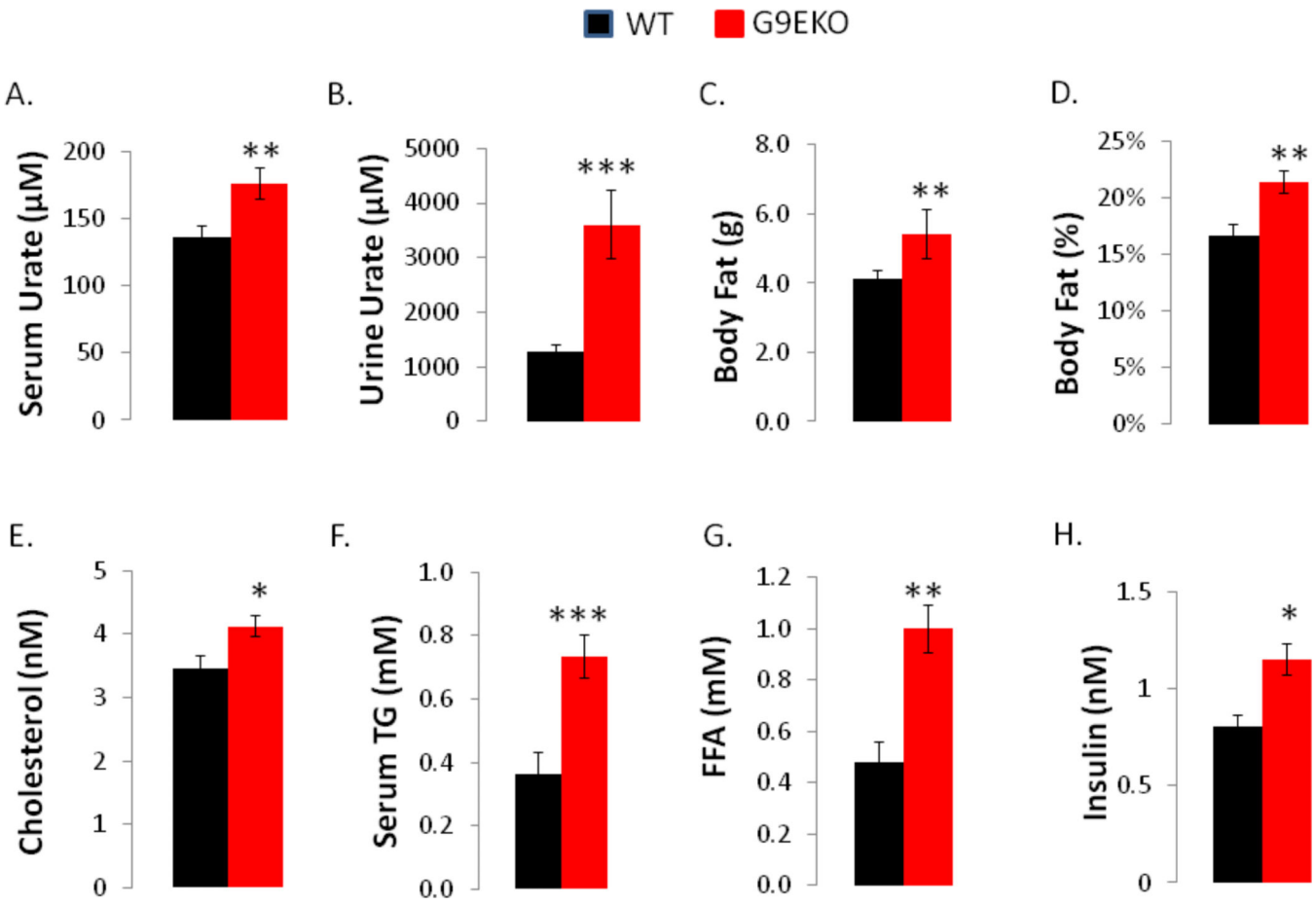

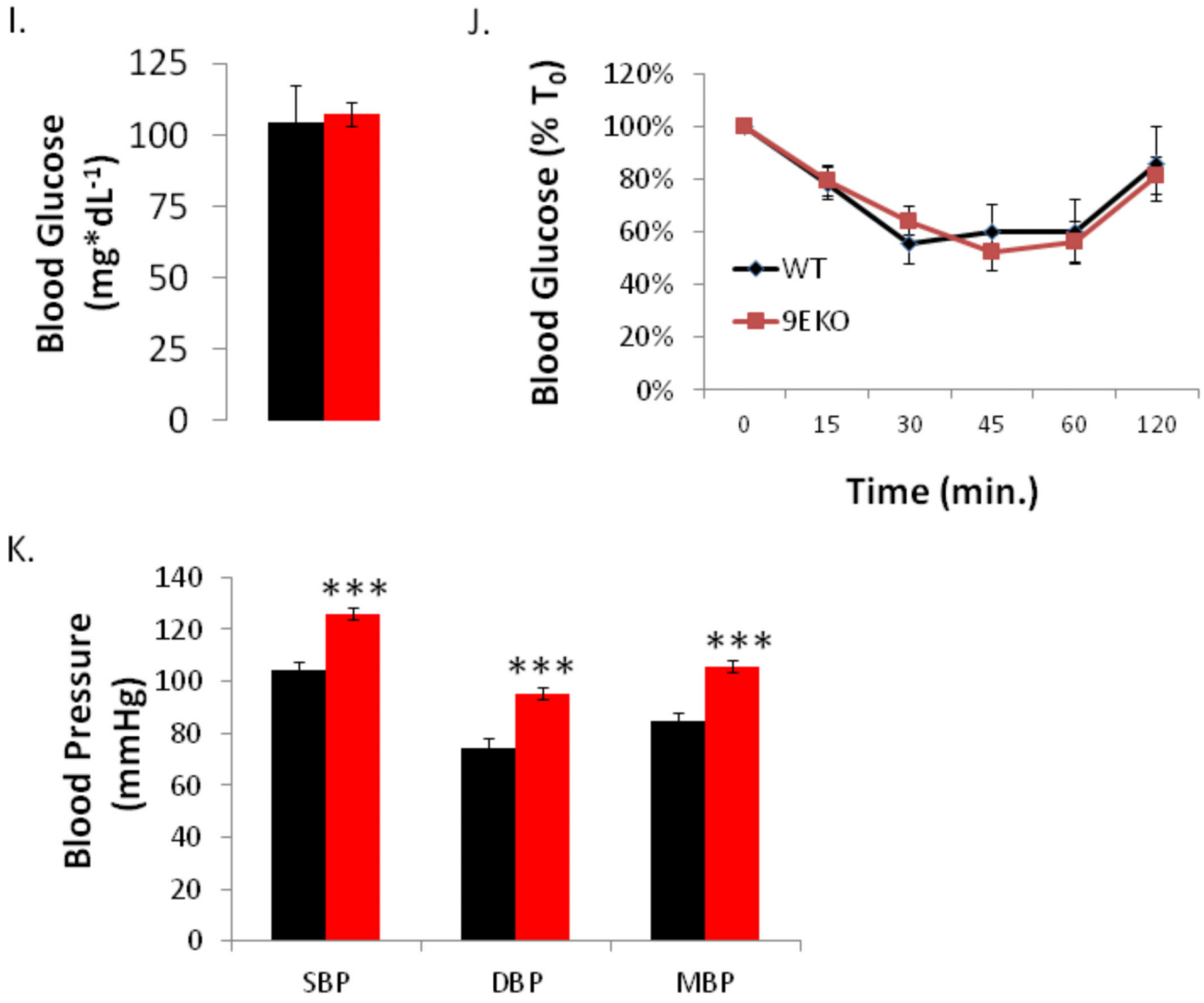

Figure 2.

Physiological consequences of enterocyte Glut9 deficiency. A. and B. Serum (n = 9, 16) and urine (n = 13, 12) uric acid concentration in fasting 6-8wk old mice. C. and D. Echo MRI analysis of fat mass and percentage fat (n = 19, 10). E. – I. Plasma cholesterol (n = 6, 5), triglycerides, free fatty acids, insulin (n = 5, 4), and glucose in fasting WT and G9EKO mice. J. Insulin tolerance testing in 4-hour fasting mice (n = 6, 22). K. Systolic (SBP), diastolic (DBP) and mean (MBP) blood pressure in non-fasting WT mice and G9EKO (n = 9, 17). *, $P < 0.05$. **, $P < 0.01$, and ***, $P < 0.001$ versus WT [2-tailed T-testing]. Error bars represent SEM.

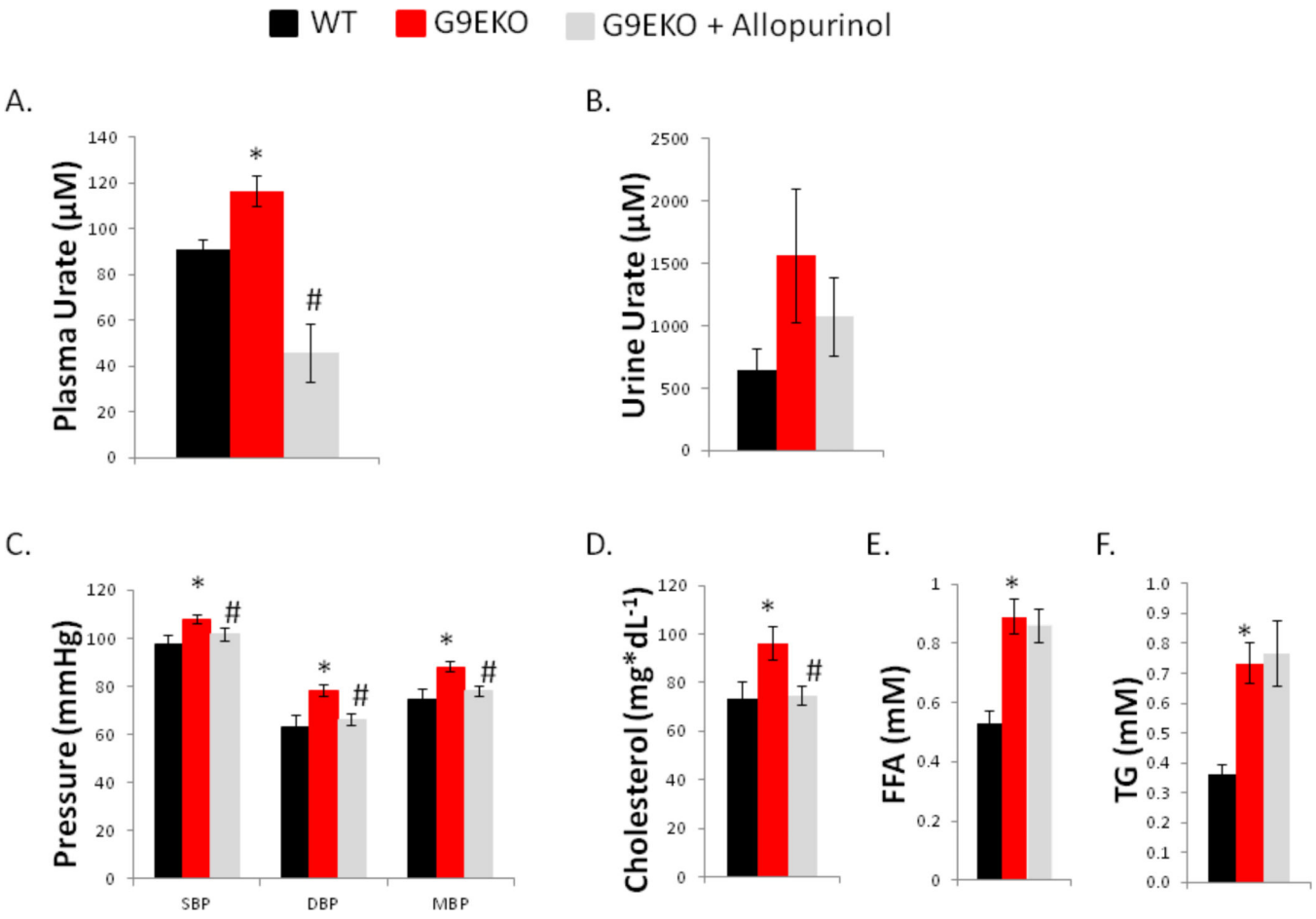

Figure 3.

Allopurinol mitigates G9EKO hyperuricemia, hypertension and dyslipidemia. A. and B. Serum (n = 8, 18, 8) and urine uric acid (n = 4, 7, 7) in WT and G9EKO fed sterile water or water containing allopurinol. C. Systolic (SBP), diastolic (DBP) and mean (MBP) blood pressure in unmedicated or in allopurinol-treated G9EKO and WT mice (n = 5, 9, 7). D., E. and F. Fasting cholesterol (n = 6, 5, 8), FFA (n = 5, 5, 5) and TG (n = 5, 5, 10) in WT and G9EKO mice. *, $P < 0.05$ versus WT. #, $P < 0.05$ versus untreated G9EKO mice [2-tailed T-testing with Bonferroni-Dunn *post hoc* correction for data sets on which multiple comparisons are made]. Error bars represent SEM.

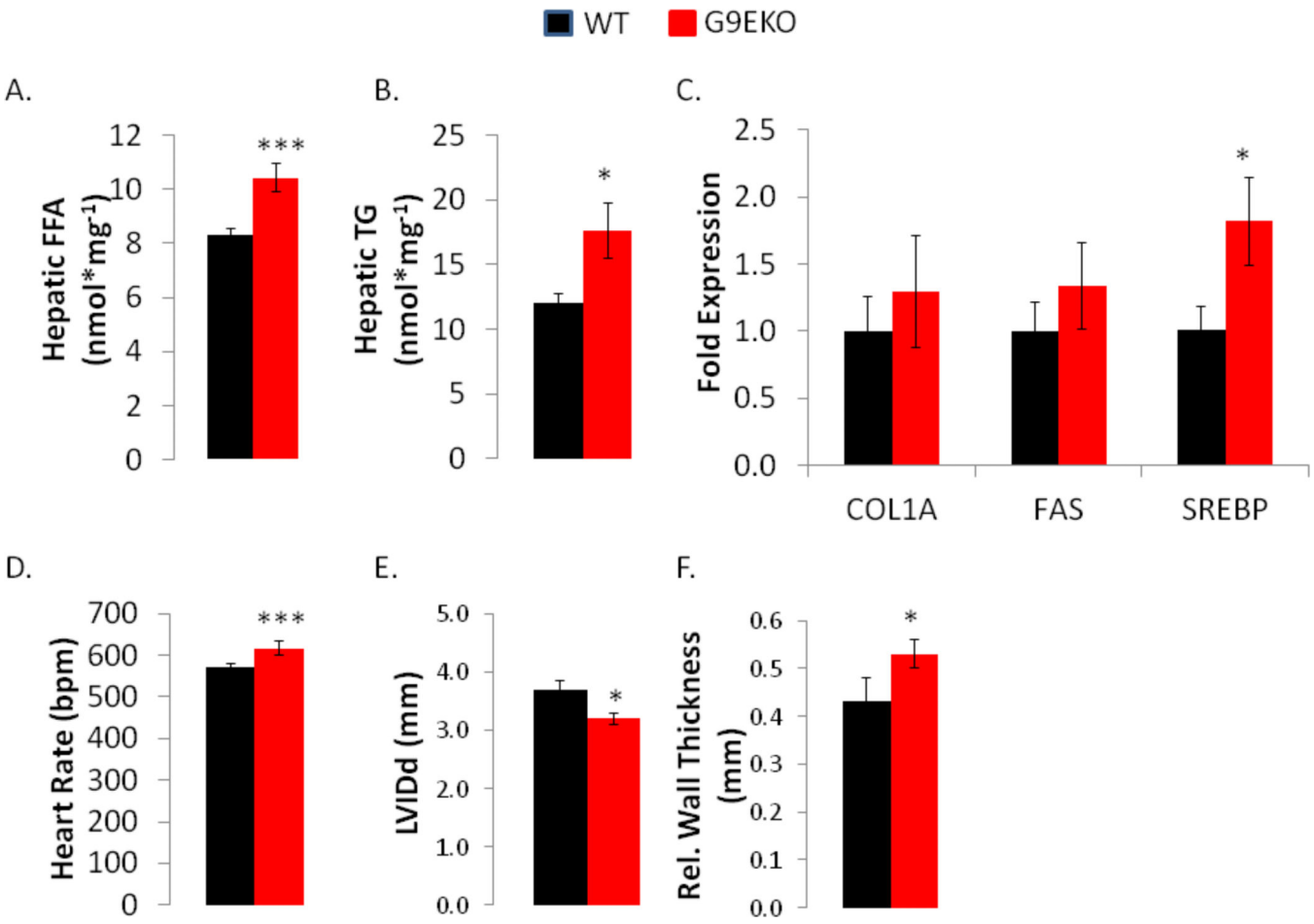

Figure 4.

Early-onset NAFLD and cardiac remodeling in G9EKO mice. A. and B. hepatic FFA (n = 6 , 6) and TG (n = 6, 6). In WT and G9EKO liver homogenates. C. Relative mRNA abundance of collagen type 1a, fatty acid synthase and sterol response element binding protein -1 by qRT-PCR analysis. D. E. and F. Echocardiographic analysis of heart rate, diastolic left ventricular internal diameter and relative wall thickness in WT and G9EKO mice (n = 5, 5). *, P < 0.05 vs. WT. ***, P < 0.001 versus WT [2-tailed T-testing]. Error bars represent SEM.

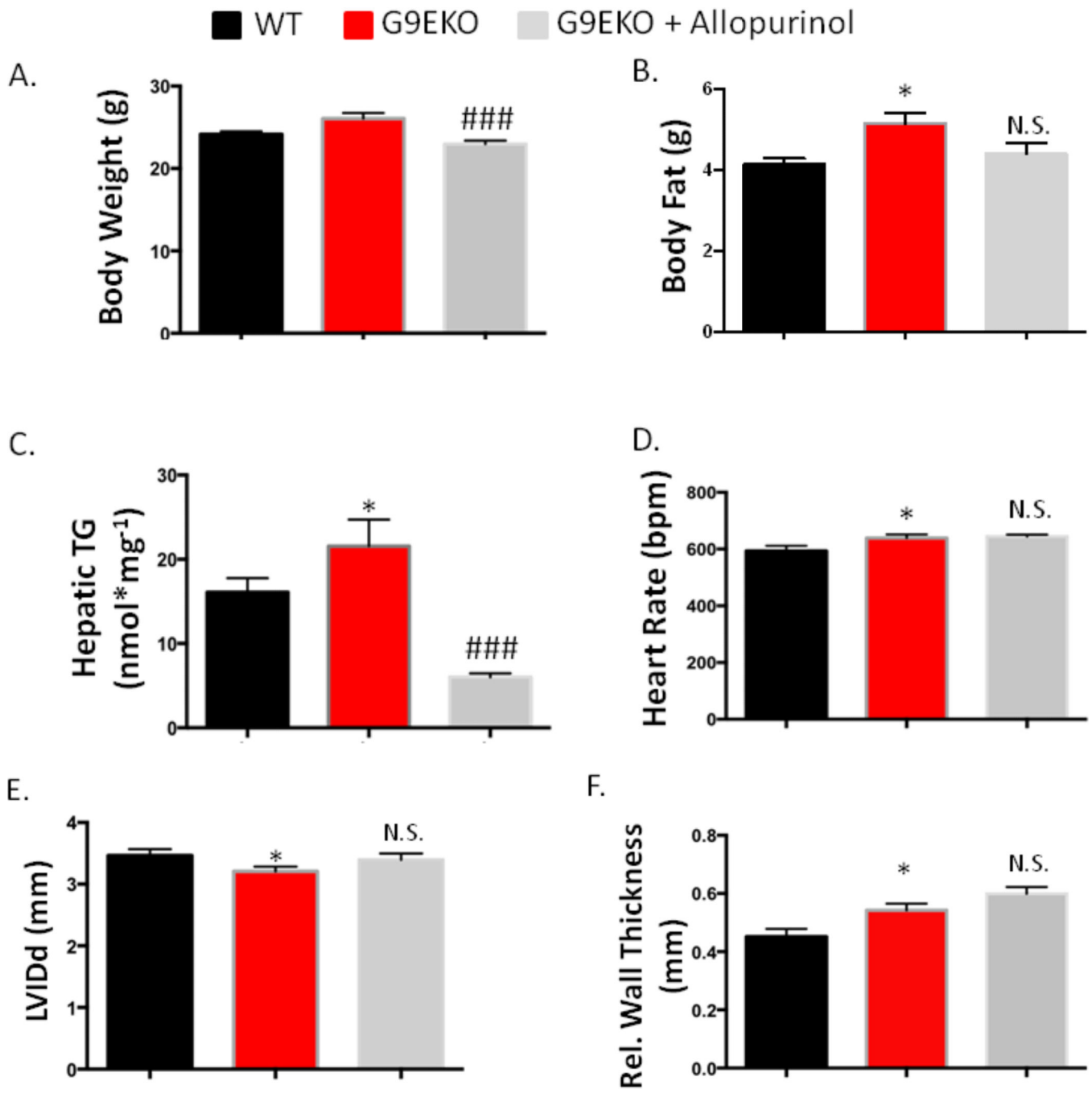

Figure 5.

Allopurinol reduces body weight and hepatic triglycerides in G9EKO mice. Shown is the effect of ~8-week allopurinol treatment (150mg / L fed *ad libitum* in water) on A) and B) body weight and body fat (n = 21, 19, 24) and C) hepatic triglycerides (TG, n = 11, 9, 7). Panels D, E, F, demonstrate the effect of allopurinol on echocardiographic parameters (n = 12, 6, 12). HR, heart rate, LVIDd, internal left ventricular diameter in diastole. RWT, relative wall thickness. *, $P < 0.05$ versus WT control by 2-tailed T-Test after Bonferroni-Dunn post-hoc correction for multiple comparisons. ###, $P < 0.001$ versus untreated G9EKO

mice. N.S., not statistically significantly different versus G9EKO untreated mice [2-tailed T-Test after Bonferroni-Dunn post-hoc correction]. Error bars represent SEM.

Table 1

Basic morphometric parameters in WT and G9EKO mice.

	n	BW	LW	HW	LW/BW	HW/BW
WT	19	24.9	952.5	132.2	39.3	5.5
G9EKO	10	26.1	922.2	129.9	40.1	5.7
P-value	-	0.116	0.585	0.741	0.634	0.439

BW, body weight. LW, liver weight. HW, heart weight. P-values are derived from 2-tailed T-tests.

Table 2

Indirect calorimetric data from 8- and 16-week-old WT and G9EKO mice.

	n	VO_2 (ml/g/hr)	VCO_2 (ml/g/hr)	RER (ratio)	HEAT (kcal/hr)
WT (8wk)	9	9.14	7.55	0.83	0.81
9EKO (8wk)	12	10.24*	7.44	0.74*	1.17*
WT (16wk)	10	8.61	7.32	0.86	0.99
9EKO (16wk)	12	9.07*	7.27	0.81	0.97

VO2, volume of inspired oxygen, VCO_2, volume of expired carbon dioxide, RER, respiratory exchange ratio.

*$P < 0.05$ versus age-matched WT control, as determined by 2-tailed T-tests.